

文章编号: 0258-7106 (2021) 03-0419-13

Doi: 10.16111/j.0258-7106.2021.03.002

胶东三山岛金矿床黄铁矿 As 富集机制及其对金成矿作用的指示*

许 杨^{1,2}, 蓝廷广^{1,2**}, 舒 磊³, 胡换龙¹, 陈应华^{1,2}, 王 洪^{1,2}

(1 中国科学院地球化学研究所, 矿床地球化学国家重点实验室, 贵州 贵阳 550081; 2 中国科学院大学地球与行星科学学院, 北京 100049; 3 山东省地质科学研究院 国土资源部金矿成矿过程与资源利用重点实验室, 山东省金属矿产成矿地质过程与资源利用重点实验室, 山东 济南 250013)

摘要 胶东是中国最大的金矿集区, 其金矿成因目前还存在较大争议。作为最重要的载金矿物, 黄铁矿显微结构及元素-同位素组成能够很好地示踪成矿物质来源和成矿过程。利用 SEM、EPMA 和 LA-ICP-MS 原位分析方法对胶东代表性蚀变岩型金矿—三山岛金矿的黄铁矿开展详细的 BSE 显微结构以及 As 含量和 S 同位素耦合关系研究, 发现矿区至少存在 3 种不同结构和 As 含量的黄铁矿: ①含金石英-黄铁矿细脉中具交代残余结构的低 As 黄铁矿(Py-1), 在 BSE 图像中显示暗色的核部(Py-1a)和亮色的边部(Py-1b), Py-1a 和 Py-1b 的 $w(\text{As})$ 分别为 $48 \times 10^{-6} \sim 524 \times 10^{-6}$ 和 $183 \times 10^{-6} \sim 1134 \times 10^{-6}$, $\delta^{34}\text{S}$ 值分别为 $10.4\text{\textperthousand} \sim 10.8\text{\textperthousand}$ 和 $11.6\text{\textperthousand} \sim 11.9\text{\textperthousand}$; ②含金石英-黄铁矿细脉中具韵律环带结构的高 As 黄铁矿(Py-2), 在 BSE 图像中显示富含矿物包裹体并多孔的核部(Py-2a)以及很少含矿物包裹体的“干净”边部(Py-2b), Py-2a 和 Py-2b 的 $w(\text{As})$ 分别为 $0.14\% \sim 0.31\%$ 和 $0.47\% \sim 0.97\%$; ③含金石英-多金属硫化物细脉中具核边结构且 As 含量变化大的黄铁矿(Py-3), 其核部 Py-3a 富含黄铜矿、闪锌矿等矿物包裹体并贫 As, $w(\text{As})$ 仅为 $1 \times 10^{-6} \sim 10 \times 10^{-6}$, $\delta^{34}\text{S}$ 值为 $4.2\text{\textperthousand} \sim 5.8\text{\textperthousand}$, 边部 Py-3b 几乎不含矿物包裹体但富 As, $w(\text{As})$ 为 $8877 \times 10^{-6} \sim 17839 \times 10^{-6}$, $\delta^{34}\text{S}$ 值为 $7.7\text{\textperthousand} \sim 10.1\text{\textperthousand}$ 。上述黄铁矿中, 从 Py-1a 到 Py-1b, $w(\text{As})$ 和 $\delta^{34}\text{S}$ 值缓慢升高, 可能主要受水岩相互作用的控制; Py-2 具韵律环带且核部多孔、多矿物包裹体, 指示了较为剧烈的流体沸腾作用; Py-3a 和 Py-3b 具有截然不同的 $w(\text{As})$ 和 $\delta^{34}\text{S}$ 值, 指示了外来富 As 流体的加入。这些过程有利于 As 和 Au 的进一步富集, 多种形式的富 As 和 Au 机制表明胶东金矿存在复杂的矿化过程和物质来源, 特别是流体在迁移过程中萃取围岩中的成矿物质不可忽视。

关键词 地球化学; 黄铁矿原位分析; 显微结构; 富 As 机制; S 同位素; 三山岛金矿; 胶东

中图分类号: P618.51

文献标识码: A

Enrichment mechanisms of arsenic in pyrite from Sanshandao gold deposit (Jiaodong Peninsula, China) and implications for gold metallogenesis

XU Yang^{1,2}, LAN TingGuang^{1,2}, SHU Lei³, HU HuanLong¹ CHEN YingHua^{1,2} and WANG Hong^{1,2}

(1 State Key Laboratory of Ore Deposit Geochemistry, Institute of Geochemistry, Chinese Academy of Sciences, Guiyang 550081, Guizhou, China; 2 College of Earth and Planetary Sciences, University of Chinese Academy of Sciences, Beijing 100049, China; 3 MNR Key Laboratory of Gold Mineralization Processes and Resources Utilization, Shandong Institute of Geological Sciences, Jinan 250013, Shandong, China)

Abstract

Jiaodong Peninsula is the largest gold Province in China. How the huge amounts of gold were accumulated

* 本文得到国家自然科学基金(编号:41873048)和国家重点研发计划(编号:2016YFC0600105)联合资助

第一作者简介 许杨, 1995 年生, 男, 硕士研究生, 主要从事矿床地球化学研究。Email: xu-yang@mail.gyig.ac.cn

** 通讯作者 蓝廷广, 1983 年生, 男, 研究员, 主要从事岩浆-热液成矿作用以及流体包裹体 LA-ICP-MS 分析方法研究。Email: lanting-guang@126.com

收稿日期 2021-02-18; 改回日期 2021-04-21。赵海杰编辑。

in such an area is still controversial. Pyrite is the most important Au-carrier mineral, the elemental and isotopic compositions of which, coupled with its microtexture, can well record the specific ore-forming processes and the origin of Au. In this study, SEM, EPMA and LA-(MC)-ICP-MS analyses were conducted on microtextures as well as As contents and S isotopic compositions of pyrite from the giant Sanshandong gold deposit. The results show that at least three types of pyrite occur: ① Low-As pyrite (Py-1) in the Au-bearing quartz-pyrite vein, which shows metasomatic relict texture. Under the BSE imaging, a dark relict core (Py-1a) is surrounded by a grey rim (Py-1b). The Py-1a has As contents of $48 \times 10^{-6} \sim 524 \times 10^{-6}$ and $\delta^{34}\text{S}$ values of $10.4\text{\%o} \sim 10.8\text{\%o}$ while the Py-1b has As contents of $183 \times 10^{-6} \sim 1134 \times 10^{-6}$ and $\delta^{34}\text{S}$ values of $11.6\text{\%o} \sim 11.9\text{\%o}$; ② High-As pyrite (Py-2) in the Au-bearing quartz-pyrite vein, which shows rhythmic zoning texture. Under the BSE imaging, the pyrite has a dark porous core containing abundant mineral inclusions (Py-2a) and a bright clean rim (Py-2b). The Py-2a and Py-2b have As contents of $0.14\text{\%} \sim 0.31\text{\%}$ and $0.47\text{\%} \sim 0.97\text{\%}$, respectively; ③ Pyrite in the Au-bearing quartz-polymetallic sulfide vein (Py-3). This pyrite is characterized by core-rim texture, showing a dark As-poor core (Py-3a) and a grey As-rich rim (Py-3b). The Py-3a and Py-3b have As contents of $1 \times 10^{-6} \sim 10 \times 10^{-6}$ and $8877 \times 10^{-6} \sim 17839 \times 10^{-6}$, $\delta^{34}\text{S}$ values of $4.2\text{\%o} \sim 5.8\text{\%o}$ and $7.7\text{\%o} \sim 10.1\text{\%o}$, respectively. The slight increase of As and $\delta^{34}\text{S}$ from Py-1a and Py-1b was most likely induced by fluid-rock interaction. The rhythmic zoning texture of Py-2, coupled with its mineral inclusion-bearing and porous core, likely suggests a fluid boiling. The contrasted As and $\delta^{34}\text{S}$ values between the Py-3a and Py-3b indicate the injection of another As-rich fluid. The above processes facilitate the As and Au to be further enriched, implying that complex ore-forming processes and multiple origins of ore-forming metals contributed to the giant gold mineralization. Especially, the fluids extracting ore-forming metals from wall rocks cannot be ignored.

Key words: geochemistry, In situ analysis of pyrite, microtexture, enrichment mechanisms of As, sulfur isotope, Sanshandao gold deposit, Jiaodong Peninsula

黄铁矿在热液矿床中普遍存在,特别是在金矿床中,为最重要的载金矿物之一,其显微结构和微量元素受流体物理化学条件影响,能够很好地记录成矿过程(Reich et al., 2005; Barker et al., 2009; Large et al., 2009; Cook et al., 2009; 2013; Deditius et al., 2014; Tanner et al., 2016)。金进入黄铁矿具有多种方式,除以包体金、裂隙金和纳米金等颗粒状态赋存在黄铁矿中外,也可以晶格替代方式进入黄铁矿晶格,或者通过电化学方式吸附到黄铁矿表面(Möller et al., 1994; Maddox et al., 1998; Simon et al., 1999a; 1999b)。大量研究表明,Au进入黄铁矿晶格与As密切相关,机制包括 $\text{As}^{1+} + \text{Au}^{1+}$ 耦合替代 $\text{S}^{2-} + \text{Fe}^{2+}$ 或 $\text{As}^{3+} + \text{Au}^{1+}$ 替代 Fe^{2+} 等(Deditius et al., 2008; 2014),而As等元素含量的变化可使黄铁矿在显微结构上显示韵律环带或者相互穿插的条带。因此,结合显微结构,研究黄铁矿中As的赋存状态及变化趋势,可以很好地反演成矿物质搬运-沉淀过程,揭示成矿机制。

胶东是中国最大的金矿集区,其不到全国0.3%的国土面积赋存了超过5000 t的金,已探明金资源量超过全国的1/4(Deng et al., 2020)。胶东金

矿以类似造山型金矿(断裂控制,成矿流体中低温、低盐度、富 CO_2)以及近乎单一的金矿化(“gold-only”,金主要赋存在黄铁矿中)为特色(Qiu et al., 2002; Fan et al., 2007; Goldfarb et al., 2014)。根据矿化类型,胶东金矿可分为蚀变岩型和石英脉型。根据热液期次,可分为石英±黄铁矿期(基本不含矿)、石英-金-黄铁矿期、石英-金-多金属硫化物期以及石英-碳酸盐期(不含矿)等(Qiu et al., 2002)。前人对胶东金矿开展了大量研究,对其地质特征、成矿时代和流体性质等已经了解的比较清楚,但对成矿物质来源及成矿过程还存在一定的争议(Goldfarb et al., 2014; 朱日祥等, 2015; Li et al., 2015; Song et al., 2015; Deng et al., 2020)。例如,望儿山、寺庄、新城等金矿主成矿阶段黄铁矿缺乏多孔结构和韵律环带,As等微量元素含量总体变化不大,指示主成矿阶段流体性质相对稳定(Yang et al., 2016; Hu et al., 2020a; 2020b),而庄子金矿黄铁矿发育多孔结构与富As的韵律环带(0.4%~3.9%)(Li et al., 2018),指示成矿过程发生过强烈的流体不混溶作用。同样,大柳行和黑岚沟的富As黄铁矿(0.4%~2.5%)记录着富

As流体的脉冲过程(Feng et al., 2018; 2020)。因此,胶东金矿的黄铁矿显微结构及As含量变化指示其具有复杂的成矿过程。三山岛金矿是胶东最具代表性的超大型蚀变岩型金矿之一,前人研究表明其发育富As黄铁矿(林祖伟等,2019; Peng et al., 2021),且S同位素组成范围宽泛(1.9‰~13‰),并在矿体局部发现富甲烷的流体包裹体(Fan et al., 2003; Wen et al., 2016),指示三山岛金矿同样具有复杂的成矿过程。

随着微区原位分析技术的发展,特别是激光剥蚀-电感耦合等离子质谱(LA-ICP-MS)分析方法,可对黄铁矿显微结构和元素-同位素组成开展微米尺度的高精度研究,使精细揭示成矿过程和成矿物质来源成为可能。因此,本文在详细的野外地质调查基础上,对三山岛金矿不同阶段的矿化样品(包括矿井及深钻样品),使用扫描电镜(SEM)、电子探针

(EPMA)以及LA-(MC)-ICP-MS微区原位分析方法,对黄铁矿显微结构、As含量以及S同位素耦合关系开展研究,从而揭示As在黄铁矿中的富集机制,为进一步理解胶东金成矿物质来源及过程提供依据。

1 地质背景

1.1 区域地质

胶东半岛位于华北克拉通东缘,主要由胶北地块和苏鲁超高压变质带组成(图1),胶北地块由北部胶北隆起和南部胶莱盆地构成。胶北地块发育大量金矿床,区域内岩石主要为前寒武纪变质基底和中生代岩浆岩,其中前寒武纪变质基底岩石包括新太古代胶东群、古元古代荆山群/分子山群和新元古代蓬莱群(Tang et al., 2007; 2008; Zhai et al., 2013),中生代岩浆岩则主要为晚侏罗世花岗岩、早白垩世花岗岩闪

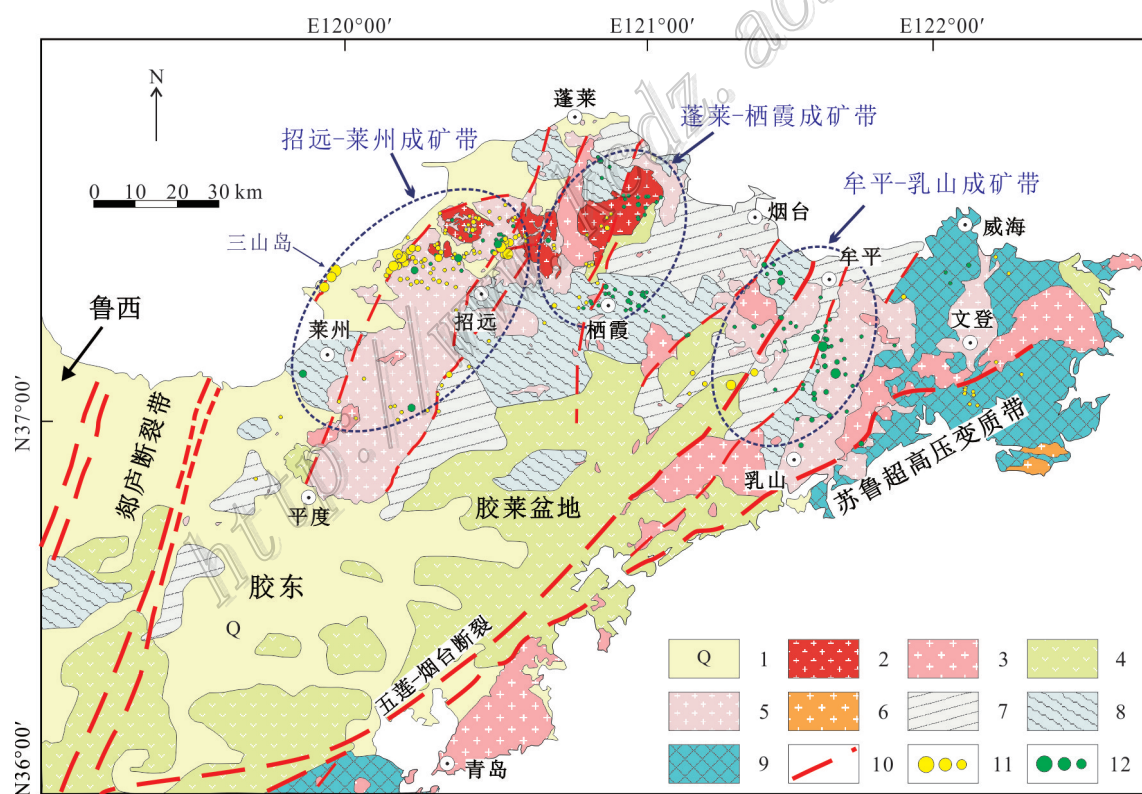


图1 胶东半岛区域地质简图(据Fan et al., 2003 和Wen et al., 2016修改)

1—第四系沉积物;2—早白垩世花岗闪长岩;3—早白垩世花岗岩;4—早白垩世火山岩;5—晚侏罗世花岗岩;6—晚三叠世侵入岩;7—古元古代荆山群/分子山群;8—新太古代胶东群;9—晚三叠世超高压变质岩;10—主要断裂;11—焦家式金矿;12—玲珑式金矿

Fig.1 Simplified regional geological map of the Jiaodong Peninsula(modified after Fan et al., 2003 and Wen et al., 2016)

1—Quaternary sediment; 2—Early Cretaceous granodiorite; 3—Early Cretaceous granite; 4—Early Cretaceous volcanics; 5—Late Jurassic granite; 6—Late Triassic intrusion; 7—Paleoproterozoic Fenzishan/Jingshan Groups; 8—Late Archean Jiaodong Group; 9—Late Triassic UHP metamorphic rock; 10—Major fault; 11—Jiaoja-type gold deposit; 12—Linglong-type gold deposit

长岩以及中-基性脉岩(Miao et al., 1997; 郭敬辉等, 2005; Hou et al., 2007; Yang et al., 2012; Cai et al., 2013)。矿体主要位于晚侏罗世花岗岩和早白垩世花岗闪长岩岩体内以及花岗岩与前寒武纪变质岩接触带。

从西向东,胶东金矿可划分为三大成矿带:招远-莱州成矿带、蓬莱-栖霞成矿带和牟平-乳山成矿带(Qiu et al., 2002; 范宏瑞等,2016)。金矿分布主要受NNE-NE向的三山岛-仓上、焦家-新城、招远-平度、牟平-乳山等断裂带控制(杨立强等,2014)。金矿主要为2种类型,即蚀变岩型和石英脉型,其中蚀变岩型金矿主要受主断裂控制,矿化呈浸染状、网脉状特征沿主断裂分布;石英脉型金矿以发育大量石英脉为特征,受区域次级断裂控制,矿体赋存于相对张性空间(Qiu et al., 2002; 杨立强等,2014; Li et al., 2015; Song et al., 2015)。

1.2 矿床地质特征

三山岛金矿位于胶东半岛西北部的招远-莱州

成矿带(图1),距莱州市~30 km,矿区探明金储量超过1000 t(宋明春等,2019),金以细脉浸染状矿化(黄铁绢英岩,蚀变岩型)为主。矿区主要由新太古代胶东群、晚侏罗世玲珑花岗岩、早白垩世郭家岭花岗闪长岩、少量基性脉岩及第四系组成。矿区断裂主要有NE走向的三山岛-仓上断裂与NW走向的三山岛-三元断裂(图2a),其中三山岛-仓上断裂为主断裂,走向NE40°~50°,倾向SE30°~40°(宋明春等,2019)。矿体主要产于玲珑花岗岩和郭家岭花岗闪长岩接触带,位于断裂下盘(图2b)。矿区内地质构造复杂,主要为I号矿体和II号矿体,其中I号矿体呈透镜状、似层状,平均品位3.96 g/t,占金矿资源>90%(Wen et al., 2016)。

主断裂面两侧围岩蚀变强烈,以断层为界限,具有明显的分带:从围岩到矿体依次为未蚀变的玲珑花岗岩/郭家岭花岗闪长岩、钾化花岗岩、绢英岩化硅化带及黄铁绢英岩带(图2b),黄铁绢英岩带与金

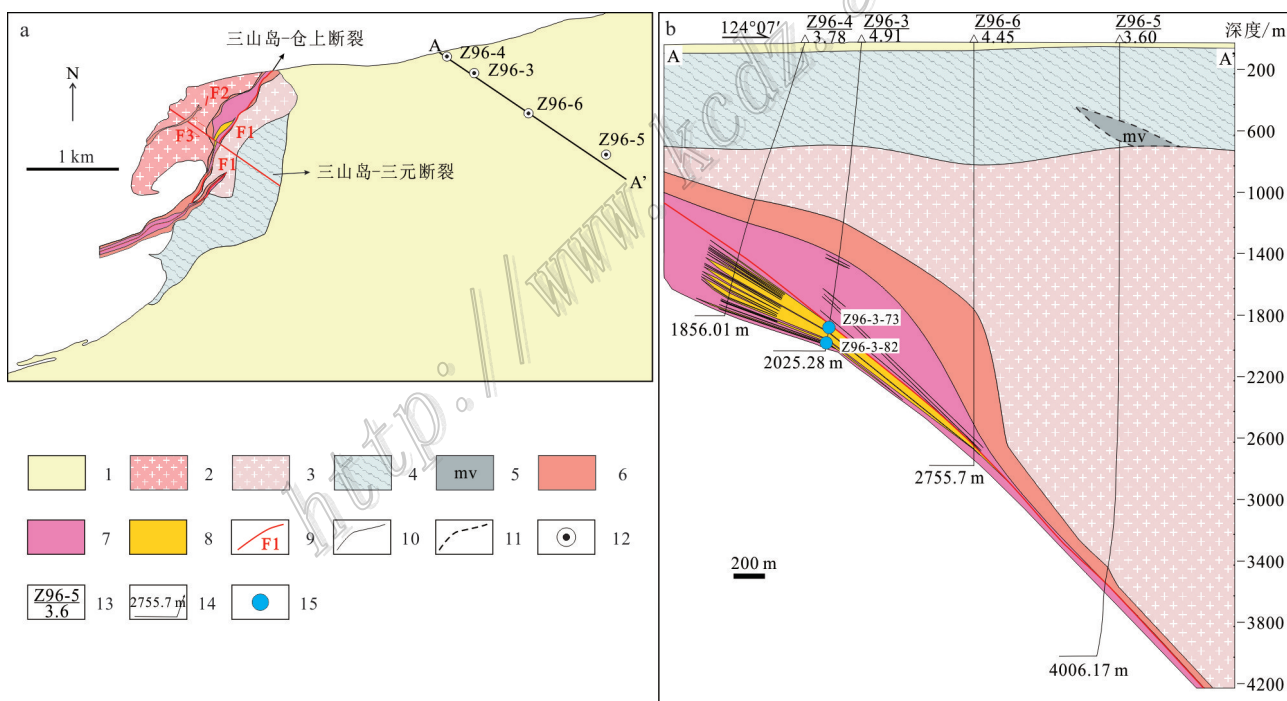


图2 三山岛金矿地质简图(a)以及三山岛金矿96 #勘探线剖面图(b)(a和b据 Wen et al., 2016 修改)

1—第四系;2—早白垩世花岗闪长岩;3—晚侏罗世花岗岩类;4—新太古代胶东群;5—变辉长岩;6—钾化带;7—绢英岩化带;8—矿体;9—断裂及编号;10—地质边界;11—推测的地质边界;12—钻孔;13—钻孔编号/海拔/m;14—钻孔深度;15—取样位置

Fig.2 Simplified geological map of the Sanshandao gold deposit (a) and geological profile along the No. 96 prospecting line in the Sanshandao gold deposit (b) (a, b modified after Wen et al., 2016)

1—Quaternary; 2—Early Cretaceous granodiorite; 3—Late Jurassic granite; 4—Late Archean Jiaodong Group; 5—Metagabbro; 6—K-feldspar alteration zone; 7—Sericitization zone; 8—Orebody; 9—Fault and its number; 10—Geological boundary; 11—Inferred geologic boundary; 12—Borehole; 13—Borehole number/elevation/m; 14—Depth of borehole; 15—Sampling location

矿化密切相关,通常即为矿体。断裂上盘主要为硅化-绢英岩化叠加于钾化,而下盘则主要为黄铁绢英岩化(矿化)叠加于早期蚀变之上(图2b)。根据热液脉穿插关系,结合矿物组合,从早到晚,大致具有白

色石英±黄铁矿期→石英-金-黄铁矿期→石英-金-多金属硫化物期→石英-碳酸盐期的演化关系(图3a、b),其中石英-金-黄铁矿期黄铁矿可呈石英+黄铁矿细脉穿插于蚀变围岩中(图3a)或呈浸染状分布于黄

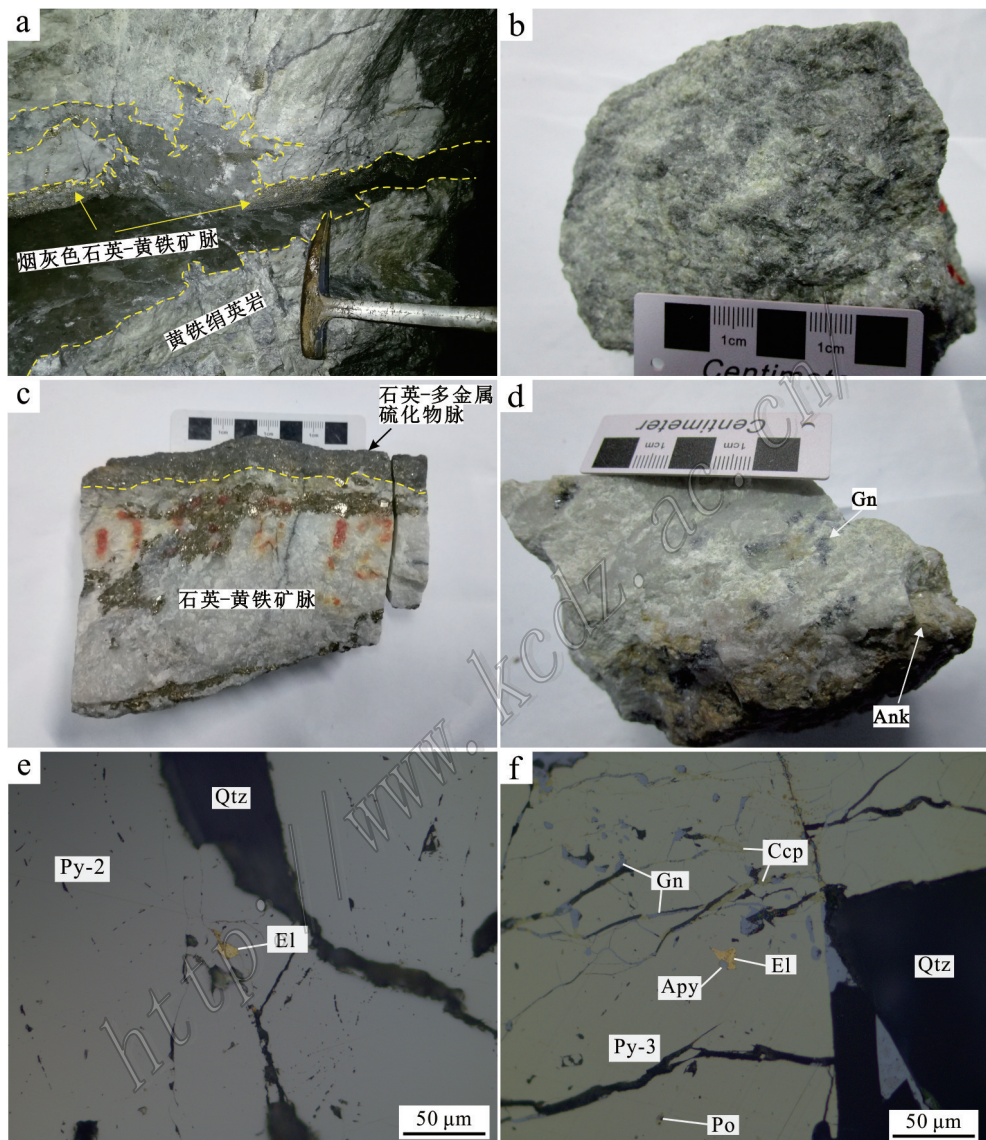


图3 三山岛金矿热液蚀变-矿化特征及不同阶段矿石矿物显微镜照片

a. 烟灰色含金石英-黄铁矿脉穿插绢英岩;b. 含金黄铁绢英岩;c. 含金石英-黄铁矿脉被石英-多金属硫化物脉穿插蚀变围岩;d. 石英-多金属硫化物脉穿插变围岩;e. 石英-金-黄铁矿阶段黄铁矿和金,金银矿位于黄铁矿裂隙中;f. 多金属硫化物阶段金银矿以包体形式赋存于黄铁矿中,金与毒砂共存,黄铁矿内同时含黄铜矿、方铅矿、磁黄铁矿及毒砂等包裹体

缩写:Ank—铁白云石;Apy—毒砂;Ccp—黄铜矿;El—金银矿;Gn—方铅矿;Py—黄铁矿;Qtz—石英

Fig. 3 Hydrothermal alteration and mineralization characteristics and microphotographs of ores from the Sanshandao gold deposit
a. Smoky Au-bearing quartz-pyrite vein crosscuts sericitic alteration zone; b. Au-bearing beresite; c. Quartz-polymetallic sulfide vein crosscuts Au-bearing quartz-pyrite vein; d. Quartz-polymetallic sulfides crosscut the altered wall rock; e. Pyrite, gold and electrum is located at the fractures of the pyrite from the quartz-gold-pyrite vein; f. Electrum occurs as mineral inclusions in the pyrite from the quartz-polymetallic sulfide vein. It coexists with arsenopyrite. Pyrite also contains polymetallic sulfides inclusions, including chalcopyrite, galena, pyrrhotite and arsenopyrite

Abbreviations: Ank—Ankerite; Apy—Arsenopyrite; Ccp—Chalcopyrite; El—Electrum; Gn—Galena; Py—Pyrite; Qtz—Quartz

铁绢英岩中(图3c)。同样,石英-金-多金属硫化物期硫化物可呈浸染状或细脉状分布于蚀变围岩中(图3d),但该阶段多种硫化物发育,包括黄铁矿、黄铜矿、磁黄铁矿、方铅矿、闪锌矿、砷黝铜矿和毒砂等。在所有矿化阶段,金主要以裂隙金或包体金赋存在黄铁矿中(图3e,f)。

2 分析方法

本次研究对不同热液阶段以及矿化深度的黄铁矿样品进行了采样和分析。样品采自三山岛矿区-120 m中段(平均品位~2 g/t)和钻孔Z96-3岩芯(采样深度为-1871 m~-1909 m,平均品位~4 g/t),包括石英-金-黄铁矿和石英-金-多金属硫化物阶段细脉。使用扫描电镜(SEM)、电子探针(EPMA)和激光剥蚀-电感耦合等离子质谱(LA-ICP-MS)分析方法对上述矿石中的黄铁矿显微结构、As含量以及S同位素进行分析,所有分析测试均在中国科学院地球化学研究所矿床地球化学国家重点实验室完成。

黄铁矿显微结构的BSE(背散射电子成像)分析在场发射扫描电镜上完成,仪器型号为日本电子JSM-7800F,配备能谱仪,实验条件为加速电压20 kV,电流10 nA。

黄铁矿的主量元素及部分微量元素测试在电子探针上完成,仪器型号为日本电子JEOL系列JXA-8230,配备能谱仪,运行条件为加速电压25 kV,电流10 nA,束斑3~10 μm(根据矿物颗粒大小而定)。计数周期为10 s的测峰时间和5 s的背景信号。数据采用ZAF方法进行校正,矿物标样为黄铁矿、镍黄铁

矿、黄铜矿、铋、毒砂、硒、金属金、金属银、辉锑矿、方铅矿,分别用于校正Fe与S、Co与Ni、Cu、Bi、As、Se、Au、Ag、Sb和Pb,数据结果列于表1。

黄铁矿微量元素LA-ICP-MS(激光剥蚀-四级杆电感耦合等离子质谱仪)分析在ASI RESOLution-LR-S155激光剥蚀系统和Agilent 7700x质谱仪上完成。激光剥蚀池为双样品池,以氦气(350 ml/min)和氩气(600 ml/min)混合气为载气。激光束斑大小为26 μm,脉冲为5 Hz,能量密度为3 J/cm²。每个采集周期包括30 s的空白和60 s的样品信号。校正方法采用多外标-内标结合法,以电子探针获得FeO含量为内标,外标GSE-1G和GSD-1G用于校正亲石元素,STDGL3用于校正亲铜元素与亲铁元素(Danyushhevsky et al., 2011)。GS系列标样推荐值来源于USGS GeoReM数据库(<http://georem.mpch-mainz.gwdg.de/>),数据分析与处理软件为LADR 1.1.2.0(<https://norsci.com/?p=ladr>; Norris et al., 2018),结果列于表2。

黄铁矿的S同位素LA-MC-ICP-MS(激光剥蚀-多接收等离子质谱仪)分析同样在上述实验室完成,使用仪器为RESOLution-LR-S155激光剥蚀系统和Nu Plasma III多接收等离子质谱仪。以氦气(350 ml/min)和氩气(800 ml/min)混合气为载气。激光束斑大小为60 μm,脉冲为5 Hz,能量密度为3 J/cm²。黄铁矿粉末压片PSPT-2为外标(Bao et al., 2017; Chen et al., 2019),实验室内部标样SB-1和HYC-1为质控外标。分析过程中获得的SB-1和HYC-1的δ³⁴S_{V-CDT}值分别为(16.7±0.7)%o和(-5.5±0.5)%o(28),与稳定同位素质谱仪获得的推荐值(SB-1为

表1 三山岛金矿黄铁矿(Py-2)电子探针主、微量元素分析结果(w(B)/%)

Table 1 EPMA major and trace element contents of pyrite(Py-2) from the Sanshandao gold deposit (w(B)/%)

点号	类型	Fe	Ni	Co	Cu	As	S	Au	Ag	Pb	Bi	总和
Z96-3-73-1	Py-2a	46.39	0.10	0.05	-	0.14	51.75	-	-	-	-	98.43
Z96-3-73-4	Py-2a	46.12	0.07	0.1	-	-	53.01	-	-	-	-	99.30
Z96-3-73-11	Py-2a	46.20	0.07	0.06	-	0.16	52.51	-	-	-	-	99.00
Z96-3-73-5	Py-2a	45.38	0.26	0.1	-	0.28	52.47	-	-	-	-	98.49
Z96-3-73-7	Py-2a	46.56	-	0.06	-	0.31	52.39	-	-	-	-	99.32
Z96-3-73-2	Py-2b	46.05	0.38	0.04	-	0.84	51.69	-	-	-	-	99.00
Z96-3-73-3	Py-2b	45.69	0.04	0.06	-	0.47	52.21	-	-	-	-	98.47
Z96-3-73-6	Py-2b	46.02	0.35	0.08	-	0.76	51.87	-	-	-	-	99.73
Z96-3-73-8	Py-2b	45.84	0.11	0.06	-	0.97	51.75	-	-	-	-	98.88
Z96-3-73-9	Py-2b	46.12	0.13	0.06	-	0.48	52.09	-	-	-	-	98.88
Z96-3-73-10	Py-2b	46.38	0.20	0.05	-	0.58	52.17	-	-	-	-	99.38

注:“-”代表低于检测限,样品采样深度为-1871 m。

16.57‰, HYC-1 为 -5.76‰) 在误差范围内一致。

3 分析结果

3.1 黄铁矿显微结构和 As 含量

根据显微结构和 As 含量, 本次研究中的黄铁矿可划分为 3 种类型:

① 低 As 黄铁矿 (Py-1), 主要发育于石英-金-黄铁矿期细脉中, 在 BSE 图像中具有明显的暗色和亮色带, 其中 Py-1a 为暗色带, 被亮色带 Py-1b 交代, 形成交代残余结构 (图 4a)。Py-1a 和 Py-1b 均没有明显的环带或韵律结构, 矿物包裹体较少, 主要为黄铜

矿。Py-1 的 As 含量低于电子探针检测限。LA-ICP-MS 分析显示, Py-1a 的 $w(\text{As})$ 为 $48 \times 10^{-6} \sim 524 \times 10^{-6}$, Py-1b 的 $w(\text{As})$ 为 $183 \times 10^{-6} \sim 1134 \times 10^{-6}$ (表 1), Py-1b 相对 Py-1a 略高, 但没有显著差别;

② 高 As 黄铁矿 (Py-2), 同样分布于石英-金-黄铁矿期细脉中, BSE 图像显示 Py-2 发育韵律环带, 其中 Py-2a 为核部暗色带, 具多孔结构, 包含硫化物和硅酸盐包裹体, 而 Py-2b 较干净, 含较少矿物包裹体 (图 4b)。电子探针分析 (Py-2 颗粒普遍较小, 未进行 LA-ICP-MS 分析) 显示 (表 1), Py-2a 的 $w(\text{As})$ 为 0.14%~0.31%, Py-2b 更富 As, $w(\text{As})$ 为 0.47%~0.97%;

③ As 含量变化大的黄铁矿 (Py-3), 主要发育于

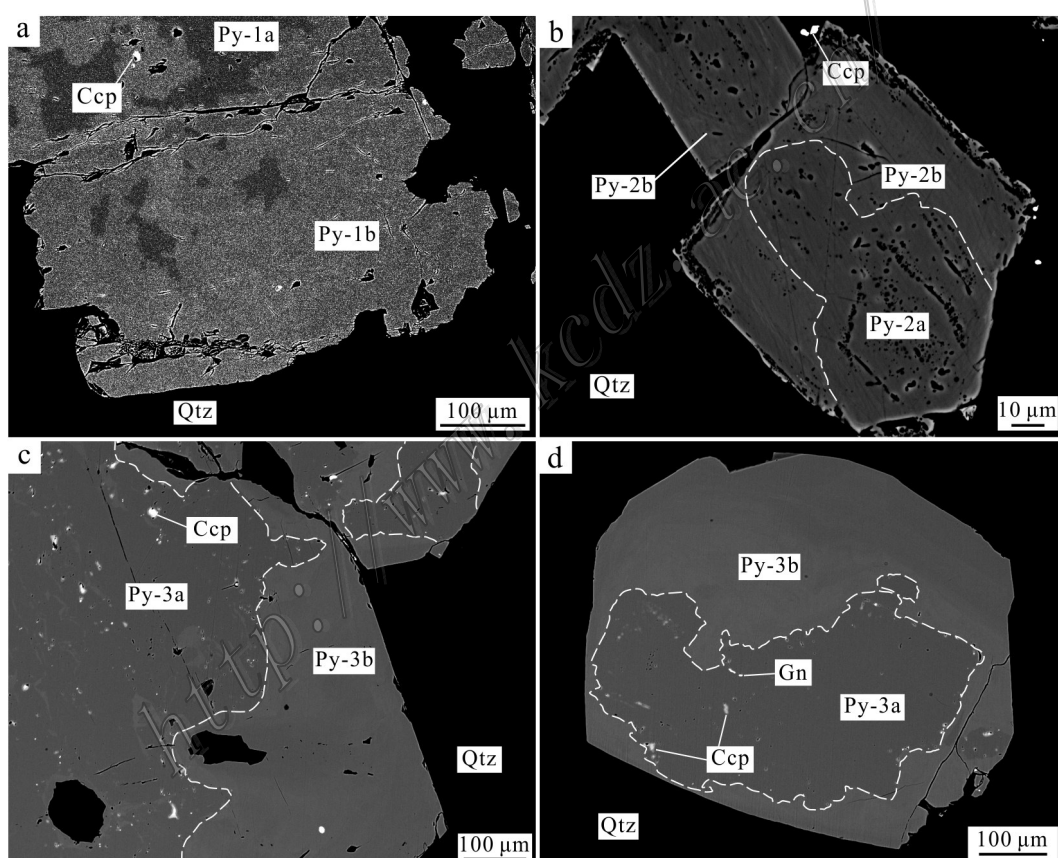


图 4 三山岛金矿具不同 As 含量及显微结构的黄铁矿 BSE 图像

a. 石英-金-黄铁矿脉中低 As 黄铁矿 Py-1, 其中 Py-1b 交代 Py-1a, 形成交代残余结构; b. 石英-金-黄铁矿脉中富 As 黄铁矿 Py-2, 显示韵律环带, 其中核部 Py-2a 具有多孔结构, 含较多矿物, Py-2b 较干净, 很少含矿物包裹体; c. 石英-金-多金属硫化物脉中 As 含量变化大的黄铁矿 Py-3, 其中 Py-3a 含大量矿物包裹体(包括黄铜矿、方铅矿和毒砂等), Py-3b 非常干净, 几乎不含矿物包裹体;

d. 基本同图 c, 但具有更明显的核边/增生结构。矿物名缩写同图 3

Fig.4 BSE images of pyrites having different As contents and microstructures from the Sanshandao gold deposit

a. Low-As pyrite (Py-1) from the Au-bearing quartz-pyrite vein, in which Py-1a is metasomatised by Py-1b; b. High-As pyrite (Py-2) from the Au-bearing quartz-pyrite vein, which shows rhythmic zoning. The Py-2a is porous and contains more mineral inclusions than the Py-2b;

c. Pyrite containing widely varied As contents (Py-3) from the Au-bearing quartz-polymetallic sulfide vein, in which Py-3a contains numerous sulfide inclusions while the Py-3b is much more clean. Abbreviations are the same as those in Fig. 3

表2 三山岛金矿黄铁矿LA-ICP-MS微量元素($w(B)/10^{-6}$)及硫同位素组成Table 2 LA-ICP-MS trace element ($w(B)/10^{-6}$) and sulfur isotopic compositions of pyrite from the Sanshando gold deposit

点号	采样深度/m	类型	Co	Ni	Cu	As	Ag	Au	Pb	Bi	$\delta^{34}\text{S}_{\text{V}-\text{CDT}}/\text{\%}$
Z96-3-82-1	-1909 m	Py-1a	-	-	-	524	-	-	0.05	0.04	10.3
Z96-3-82-2		Py-1a	-	-	12.5	523	7.39	0.12	31.5	34.9	10.8
Z96-3-82-3		Py-1a	0.05	-	-	48.5	-	-	0.13	-	10.4
Z96-3-82-4		Py-1b	1.76	0.5	5.41	1134	7.64	0.17	73.1	42.7	11.6
Z96-3-82-5		Py-1b	-	0.21	2.76	183	1.93	0.14	6.91	7.47	11.9
Z96-3-82-6		Py-1b	-	0.86	10.7	185	2.02	0.04	48.6	10.2	11.6
17SSD01-3		Py-3a	1.64	0.39	-	1.11	-	-	0.74	0.02	5.8
17SSD01-4		Py-3a	0.51	0.56	12.3	9.54	0.84	-	2.51	-	4.2
17SSD01-1	-120 m	Py-3b	5.04	0.94	-	8877	-	0.48	1.10	-	8.8
17SSD01-2		Py-3b	0.40	0.54	0.82	12238	-	0.75	1.18	-	7.7
17SSD01-5		Py-3b	12.6	125	0.80	17839	-	1.16	0.06	-	10.1

注:“-”代表低于检测限。

多金属硫化物脉中,在BSE图像中显示核边结构,其中Py-3a为核部暗色带,含较多硫化物包裹体(如黄铜矿、闪锌矿、方铅矿等);Py-3b边部带,相对较亮,结构均一,很少含矿物包裹体(图4c,d)。LA-ICP-MS分析显示,Py-3a贫As, $w(\text{As})$ 为 $1\times 10^{-6}\sim 10\times 10^{-6}$,而Py-3b富As, $w(\text{As})$ 为 $8877\times 10^{-6}\sim 17\ 839\times 10^{-6}$ (表2)。

3.2 黄铁矿微区S同位素特征

因Py-2颗粒较小,未能进行LA-MC-ICP-MS硫同位素分析。Py-1a的 $\delta^{34}\text{S}$ 值为 $10.4\text{\%}\sim 10.8\text{\%}$,Py-1b为 $11.6\text{\%}\sim 11.9\text{\%}$,后者略高,但没有显著差别(表1)。Py-3a的 $\delta^{34}\text{S}$ 值为 $4.2\text{\%}\sim 5.8\text{\%}$,Py-3b的 $\delta^{34}\text{S}$ 值为 $7.7\text{\%}\sim 10.1\text{\%}$,二者相差较大(表2)。

4 讨 论

4.1 黄铁矿显微结构与As富集机制

黄铁矿显微结构受控于多种因素,包括元素的分布以及结晶条件等(Reich et al., 2005; Large et al., 2007; Cook et al., 2009; Deditius et al., 2014; Peterson et al., 2014; Román et al., 2019; Hu et al., 2020b)。如As、Co、Ni和Cu等元素在黄铁矿中的含量通常较高,可造成黄铁矿在BSE图像中显示不同环带/条带(Reich et al., 2013)。不同的结晶条件同样可以造成黄铁矿的不同显微结构,如对地热系统中的黄铁矿研究表明,在较为稳定的生长条件下,黄铁矿晶型通常为自形-半自形,很少发育多孔结构和矿物包裹体,相对富Co、Ni,贫As、Au、Ag、Cu和Pb,而在沸腾

条件下,黄铁矿为自形-他形,具有多孔结构和矿物包裹体,富As、Au、Ag、Cu和Pb,贫Co和Ni,这归因于沸腾环境下物理-化学条件的剧烈变化(Román et al., 2019)。

本研究中,Py-1a和Py-1b均没有明显的环带结构,矿物包裹体也较少,表明结晶环境较为稳定,在BSE图像中较大的亮度差异可能是由不同成分引起的,这得到As含量和S同位素组成的支持。从Py-1a到Py-1b, $w(\text{As})$ 从 $48\times 10^{-6}\sim 524\times 10^{-6}$ 变化至 $183\times 10^{-6}\sim 1134\times 10^{-6}$, $\delta^{34}\text{S}$ 值从 $10.4\text{\%}\sim 10.8\text{\%}$ 变化至 $11.6\text{\%}\sim 11.9\text{\%}$,具有轻微的升高(图5a~c)。轻微的升高指示了相对稳定的过程,结合Py-1a和Py-1b之间的交代残余关系,一个可能的过程是,Py-1在沉淀过程中,早期沉淀的Py-1a被后期不断演化的热液交代,形成Py-1b,由于后期热液经历了更多的水岩相互作用,热液中的As含量和 $\delta^{34}\text{S}$ 值逐渐升高,导致Py-1b具有相对较高的As和 $\delta^{34}\text{S}$ 值。事实上,含矿热液通过水岩相互作用导致As甚至Au等元素含量以及S同位素组成的升高在热液金矿中常见,特别是在卡林型金矿中(Ilchik et al., 1997; Emsbo et al., 2003; 2006; Cline et al., 2005; Kesler et al., 2005; Large et al., 2011)。因此,Py-1中As含量的变化可能受控于较为持续且稳定的水岩相互作用。

Py-2发育韵律环带,特别是核部的Py-2a显示多孔结构并包含大量矿物包裹体(图4b),与典型沸腾条件下沉淀的黄铁矿具有很大的相似性,暗示其可能形成于沸腾条件下的快速沉淀,沉淀过程中物理化学条件(如压力)的振荡变化可导致黄铁矿韵律条

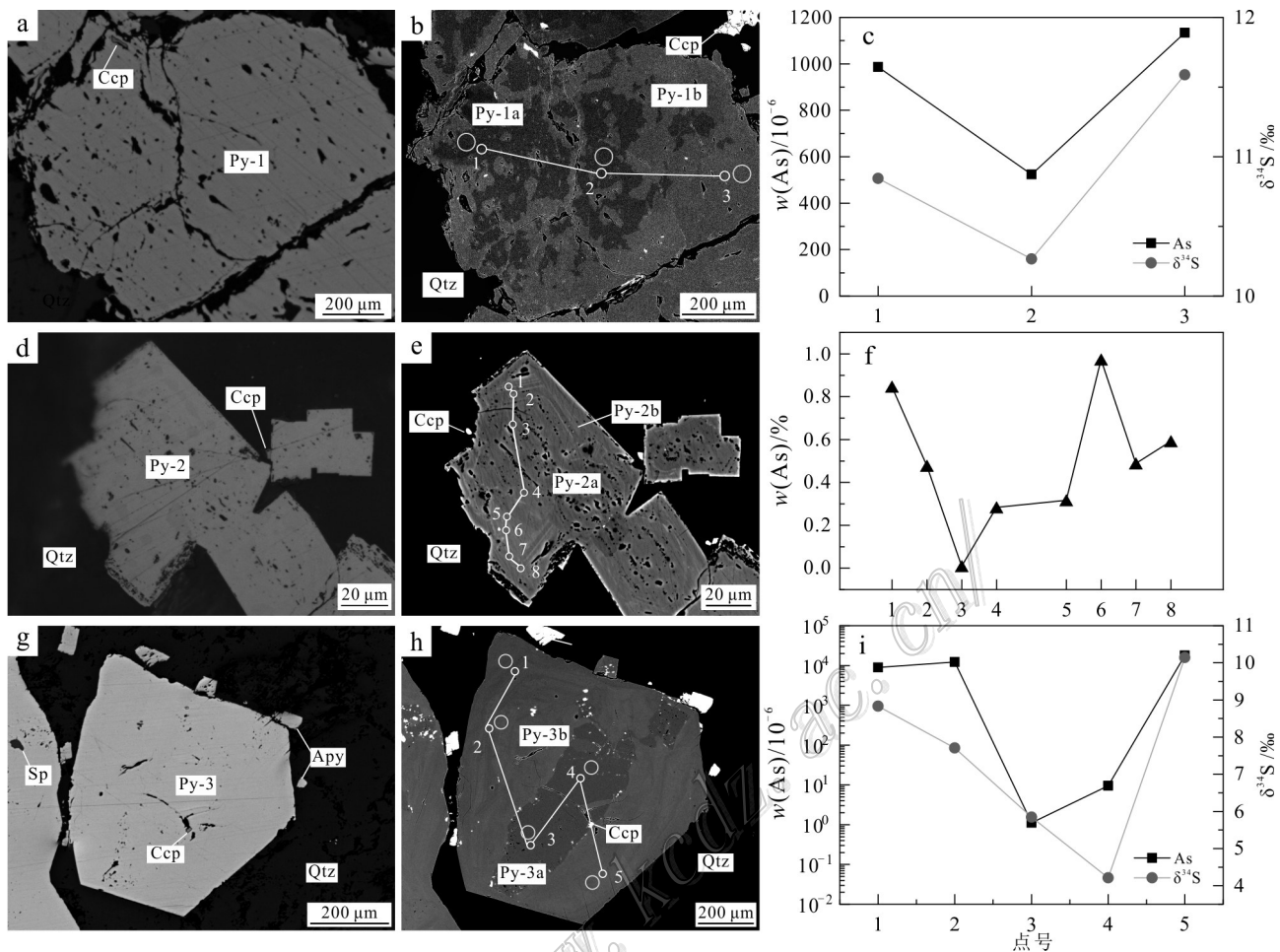


图5 三山岛金矿不同类型黄铁矿显微结构与As含量及S同位素组成协变图

a. 石英-金-黄铁矿脉中的Py-1光学显微照片;b. 图5a中Py-1的BSE图像及As含量和S同位素打点位置;c. 图5b中Py-1的As含量与 $\delta^{34}\text{S}$ 值关系图;d. 石英-金-黄铁矿脉中Py-2的显微照片;e. 图5d中Py-2的BSE图像及As含量打点位置;f. 图5e中Py-2的As含量变化图;g. 石英-金-多金属硫化物脉中Py-3的显微照片;h. 图5g中Py-3的BSE图像及As含量和S同位素打点位置;i. 图5h中Py-3的As含量和 $\delta^{34}\text{S}$ 值关系图。图5b,e和h中,小圈为微量元素分析点位置,大圈为硫同位素分析点位置。矿物名缩写同图3

Fig.5 The covariations among microtextures, As contents and $\delta^{34}\text{S}$ values of different types of pyrite from the Sanshandao gold deposit

a. Optical microphotograph of Py-1 from quartz-Au-pyrite vein; b. BSE image and analytical positions of As contents and $\delta^{34}\text{S}$ values of Py-1 in Fig.5a; c. Plot of As contents and sulfur isotopic compositions of Py-1 in Fig.5b; d. Optical microphotograph of Py-2 from quartz-Au-pyrite vein; e. BSE image and analytical positions of As contents of Py-2 in Fig.5d; f. Plot of EPMA As contents of Py-2 in Fig.5e; g. Optical microphotograph of Py-3 from quartz-Au-polymetallic sulfide vein; h. BSE image and analytical positions of As contents and $\delta^{34}\text{S}$ values of Py-3 in Fig.5g; i. Plot of As contents and $\delta^{34}\text{S}$ values of Py-3 in Fig.5h. In Fig.5b, e and h, the small circles represent the analytical spots of trace elements, and the big circles represent the analytical spots of sulfur isotopic analysis. The abbreviations are the same as those in Fig. 3

带的形成(Velasquez et al., 2014)。另外,沸腾作用可能导致多种元素在早期沉淀(Román et al., 2019),随着时间演化热液变得更“纯”,沉淀出来的黄铁矿杂质较少,从而形成较为“干净”的Py-2b(图4b)。Py-2a和Py-2b的As含量均较高,分别为0.14%~0.31%和0.47%~0.97%(表1),从Py-2a到Py-2b具有

升高的趋势(图5d~f),表明初始富As流体并随着时间演化As更为富集。研究表明,黄铁矿中的As含量与温度密切相关,温度越高,As含量越低(Deditius et al., 2014; Xing et al., 2019)。反之,随着温度的降低,更多的As进入黄铁矿晶格,从而形成更富As的黄铁矿。因此,从Py-2a到Py-2b,As含量的升

高可能与流体演化过程中温度的降低有关,即早期相对具较高温度的流体发生沸腾,形成多孔、多矿物包裹体的Py-2a,随着能量的消耗(温度的降低)及沸腾作用的结束,As更多进入黄铁矿,形成更富As且“干净”的Py-2b。沸腾作用伴随流体温度、压力降低是热液演化过程中常有的现象,上述现象在胶东其他金矿也有发现,如Li等(2018)在庄子金矿发现黄铁具有多孔结构,显示As的韵律环带($w(\text{As})$ 为0.4%~3.9%),指示成矿过程发生过强烈的流体不混溶过程,压力变化导致局部流体相分离。因此,Py-2中韵律结构和As的变化可能源自沸腾作用和温度下降的协同控制。

Py-3具核边结构,核部Py-3a含较多矿物包裹体而边部Py-3b较为“干净”(图4c,d),同时Py-3a和Py-3b在As含量和 $\delta^{34}\text{S}$ 值方面具有显著差异(图5g~i),Py-3a贫As($w(\text{As})$ 为 $1 \times 10^{-6} \sim 10 \times 10^{-6}$)、低 $\delta^{34}\text{S}$ 值(4.2‰~5.8‰),Py-3b富As($w(\text{As})$ 为 $8877 \times 10^{-6} \sim 17839 \times 10^{-6}$)、高 $\delta^{34}\text{S}$ 值(7.7‰~10.1‰),明显指示了两期不同的流体。贫As、低 $\delta^{34}\text{S}$ 值的流体特征与胶西北多数金矿的成矿期流体相似,而富As、高 $\delta^{34}\text{S}$ 值则相对较少,但最近也在胶东一些金矿中被识别出来。如Feng等(2018;2020)发现胶东黑岗沟、大柳行等金矿中存在富As($w(\text{As})$ 为0.4%~2.5%)、高 $\delta^{34}\text{S}$ 值(>8‰)黄铁矿,提出成矿流体在迁移过程中与富As的变沉积岩发生了水岩相互作用,萃取了其中的S和As而变得更富集。因此,Py-3b中As的富集最有可能受控于外部富As流体的加入。

以上结果表明,三山岛矿区黄铁矿中至少存在3种As富集机制,一是通过持续的水岩相互作用使流体缓慢富集As,从中沉淀的黄铁矿因而逐渐富As,这与三山岛金矿主要为蚀变岩型矿化的地质特征相符;二是通过沸腾作用、温度下降等相对快速的过程使As富集在相对晚期沉淀的黄铁矿中。大量地质现象表明,蚀变岩型金矿尽管以蚀变岩型矿化为主,但局部地方也可存在石英脉型矿化(如邻近的焦家金矿新Ⅲ号矿体),这可能与不同构造部位的应力变化有关,在相对张性构造部位可发生流体沸腾作用;三是外来富As流体的注入。机制一指示成矿流体可能萃取围岩中的成矿元素变得更富集,这可在蚀变岩型矿化中普遍发生,机制二代表了相对剧烈的过程,可能在石英脉型矿化中更容易发生,机制三在蚀变岩和石英脉型矿化中均可发生,依赖于外来流体的性质。

4.2 对金矿化作用的指示

胶东金矿成矿流体为中低温(主要250~

350 °C)、低盐度($w(\text{NaCl}_{\text{eq}}) < 10\%$)、富CO₂流体(Qiu et al., 2002; Fan et al., 2007; Goldfarb et al., 2014),Au可能主要以Au(HS)₂络合物形式迁移(Benning et al., 1996; Stefansson et al., 2004; Williams-Jones et al., 2009; Yang et al., 2016)。Py-1a和Py-1b呈交代残余结构,在很大程度上指示了一个持续的水岩相互作用过程,这与蚀变岩型矿化机制一致,水岩相互作用引起物理化学条件变化,导致Au(HS)₂络合物失稳,从而沉淀Au。Py-2a和Py-2b显示韵律环带,Py-2a呈多孔结构和并且富含矿物包裹体,可能指示了压力/温度变化引起的流体沸腾,其代表了较为剧烈的物理化学条件变化,这种变化导致Au(HS)₂络合物快速失稳,有利于金沉淀,这在石英脉型矿化环境更容易发生。Py-3a与Py-3b代表了2种不同的成矿流体,指示胶东金矿成矿物质不是单一来源,可能包含了一个统一的深部来源以及流体迁移过程中围岩物质的贡献。上述过程对As具有再富集作用,而As与Au密切相关(图6),As的富集可造成Au的富集,有利于提高Au的品位。值得强调的是,本次研究显示As最重要的富集可能与成矿流体对围岩的萃取有关,这暗示围岩中的Au对胶东金矿的贡献可能不可忽视,需要引起重视。

5 结 论

(1) 三山岛金矿黄铁矿存在3种代表性显微结构,包括交代残余结构、韵律环带结构和核边结构。

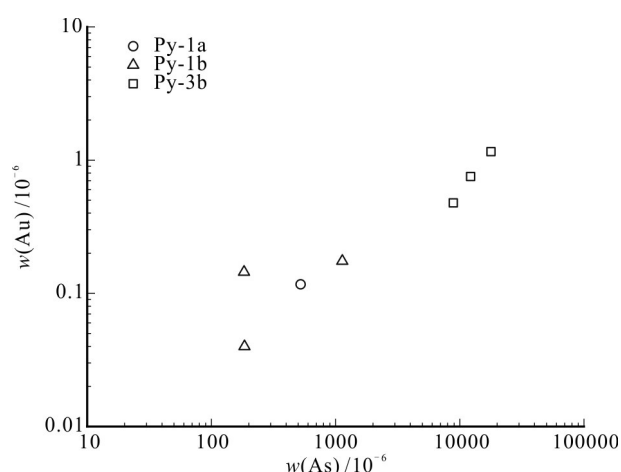


图6 三山岛金矿黄铁矿中As和Au协变图

Fig. 6 Correlation between As and Au in pyrite from the Shanshandao gold deposit

(2) 三山岛金矿黄铁矿至少存在3种As再富集过程:水岩相互作用、流体沸腾伴随温度下降以及外来富As流体的加入。

(3) 多种形式的富As机制表明胶东金矿存在复杂的矿化过程和物质来源,特别是流体萃取围岩中的成矿物质不可忽视,蚀变岩型和石英脉型矿化Au沉淀方式可能存在差异。

致 谢 感谢矿床地球化学国家重点实验室董少花、郑文勤和李响以及戴智慧、陈佑伟和张雪分别在矿物BSE分析、EMPA测试以及LA-ICP-MS微量元素以及S同位素分析方面提供的帮助。感谢两名审稿人提出的宝贵意见和建议。

References

- Bao Z A, Chen L, Zong C L, Yuan H L, Chen K Y and Dai M L. 2017. Development of pressed sulfide powder tablets for in situ sulfur and lead isotope measurement using LA-MC-ICP-MS[J]. International Journal of Mass Spectrometry, 421: 255-262.
- Barker S L L, Hickey K A, Cline J S, Dipple G M, Kilburn M R, Vaughan J R and Longo A A. 2009. Uncloaking invisible gold: Use of NanoSIMS to evaluate gold, trace elements, and sulfur isotopes in pyrite from Carlin-type gold deposits[J]. Econ. Geol., 104(7): 897-904.
- Benning L G and Seward T M. 1996. Hydrosulphide complexing of Au(I) in hydrothermal solutions from 150~400°C and 500~1500 bar[J]. Geochimica et Cosmochimica Acta, 60(11): 1849-1871.
- Cai Y C, Fan H R, Santosh M, Liu X, Hu F F, Yang K F, Lan T G, Yang Y H and Liu Y S. 2013. Evolution of the lithospheric mantle beneath the southeastern North China Craton: Constraints from mafic dikes in the Jiaobei terrain[J]. Gondwana Research, 24(2): 601-621.
- Cline J S, Hofstra A H, Muntean J L, Tosdal R M and Hickey K A. 2005. Carlin-type gold deposits in Nevada: Critical geologic characteristics and viable models[J]. Economic Geology 100th Anniversary Volume, 451-484.
- Cook N J, Ciobanu C L and Mao J W. 2009. Textural control on gold distribution in As-free pyrite from the Dongping, Huangtuliang and Houguo gold deposits, North China Craton (Hebei Province, China)[J]. Chemical Geology, 264(1-4): 101-121.
- Cook N J, Ciobanu C L, Meria D, Silcock D and Wade B. 2013. Arsenopyrite-pyrite association in an orogenic gold ore: Tracing mineralization history from textures and trace elements[J]. Econ. Geol., 108(6): 1273-1283.
- Danyushevsky L, Robinson P, Gilbert S, Norman M, Large R, McGoldrick P and Shelley M. 2011. Routine quantitative multi-element analysis of sulphide minerals by laser ablation ICP-MS: Standard development and consideration of matrix effects[J]. Geochemistry: Exploration Environment Analysis, 11(1): 51-60.
- Deditius A P, Reich M, Kesler S E, Utsunomiya S, Chrysoulis S L, Walshe J and Ewing R C. 2014. The coupled geochemistry of Au and As in pyrite from hydrothermal ore deposits[J]. Geochimica et Cosmochimica Acta, 140: 644-670.
- Deditius A P, Utsunomiya S, Renock D, Ewing R C, Ramana C V, Becker U and Kesler S E. 2008. A proposed new type of arsenian pyrite: Composition, nanostructure and geological significance[J]. Geochimica et Cosmochimica Acta, 72(12): 2919-2933.
- Deng J, Yang L Q, Groves D I, Zhang L, Qiu K F and Wang Q F. 2020. An integrated mineral system model for the gold deposits of the giant Jiaodong Province, eastern China[J]. Earth-Science Reviews, 208: 103274.
- Emsbo P, Hofstra A H, Lauha E A, Griffin G L and Hutchinson R W. 2003. Origin of high-grade gold ore, source of ore fluid components, and genesis of the Meikle and neighboring Carlin-type deposits, northern Carlin trend, Nevada[J]. Econ. Geol., 98(6): 1069-1105.
- Emsbo P, Groves D I, Hofstra A H and Bierlein F P. 2006. The giant Carlin gold Province: A protracted interplay of orogenic, basinal, and hydrothermal processes above a lithospheric boundary[J]. Mineralium Deposita, 41: 517-525.
- Fan H R, Zhai M G, Xie Y H and Yang J H. 2003. Ore-forming fluids associated with granite-hosted gold mineralization at the Sanshan-dao deposit, Jiaodong gold Province, China[J]. Mineralium Deposita, 38: 739-750.
- Fan H R, Hu F F, Yang J H and Zhai M G. 2007. Fluid evolution and large-scale gold metallogeny during Mesozoic tectonic transition in the Jiaodong Peninsula, eastern China[J]. Geological Society, London, Special Publications, 280: 303-316.
- Fan H R, Feng K, Li X H, Hu F F and Yang K F. 2016. Mesozoic gold mineralization in the Jiaodong and Korean peninsulas[J]. Acta Petrologica Sinica, 32(10): 3225-3238 (in Chinese with English abstract).
- Feng K, Fan H R, Groves D I, Yang K F, Hu F F, Liu X and Cai Y C. 2020. Geochronological and sulfur isotopic evidence for the genesis of the post-magmatic, deeply sourced, and anomalously gold-rich Dalihuang orogenic deposit, Jiaodong, China[J]. Mineralium Deposita, 55: 293-308.
- Feng K, Fan H R, Hu F F, Yang K F, Liu X, Shangguan Y N, Cai Y C and Jiang P. 2018. Involvement of anomalously As-Au-rich fluids in the mineralization of the Heilan'gou gold deposit, Jiaodong, China: Evidence from trace element mapping and in-situ sulfur isotope composition[J]. Journal of Asian Earth Sciences, 160: 304-321.
- Goldfarb R J and Santosh M. 2014. The dilemma of the Jiaodong gold deposits: Are they unique[J]? Geoscience Frontiers, 5(2): 139-153.
- Guo J H, Chen F K, Zhang X M, Siebel W and Zhai M G. 2005. Evolution of syn- to post-collisional magmatism from north Sulu UHP

- belt, eastern China: Zircon U-Pb geochronology[J]. *Acta Petrologica Sinica*, 21(4): 1281-1301(in Chinese with English abstract).
- Hou M L, Jiang Y H, Jiang S Y, Ling H F and Zhao K D. 2007. Contrasting origins of late Mesozoic adakitic granitoids from the northwestern Jiaodong Peninsula, East China: Implications for crustal thickening to delamination[J]. *Geological Magazine*, 144 (4): 619-631.
- Hu H L, Fan H R, Liu X, Cai Y C, Yang K F and Ma W D. 2020a. Two-stage gold deposition in response to H_2S loss from a single fluid in the Sizhuang deposit (Jiaodong, China)[J]. *Ore Geology Reviews*, 120: 103450.
- Hu H L, Fan H R, Santosh M, Liu X, Cai Y C and Yang K F. 2020b. Ore-forming processes in the Wang'ershans gold deposit (Jiaodong, China): Insight from microtexture, mineral chemistry and sulfur isotope compositions[J]. *Ore Geology Reviews*, 123: 103600.
- Ilchik R P and Barton M D. 1997. An amagmatic origin of Carlin-type gold deposits[J]. *Economic Geology and the Bulletin of the Society of Economic Geologists*, 92(3): 269-288.
- Kesler S E, Riciputi L C and Ye Z. 2005. Evidence for a magmatic origin for Carlin-type gold deposits: Isotopic composition of sulfur in the Betze-Post-Screamer Deposit, Nevada, USA[J]. *Mineralium Deposita*, 40: 127-136.
- Large R R, Danyushevsky L, Hollit C, Maslennikov V, Meffre S, Gilbert S, Bull S, Scott R, Emsbo P, Thomas H, Singh B and Foster J. 2009. Gold and trace element zonation in pyrite using a laser imaging technique: Implications for the timing of gold in orogenic and Carlin-style sediment-hosted deposits[J]. *Econ. Geol.*, 104(5): 635-668.
- Large R R, Maslennikov V V, Robert F, Danyushevsky L V and Chang Z S. 2007. Multistage sedimentary and metamorphic origin of pyrite and gold in the giant Sukhoi Log deposit, Lena gold Province, Russia[J]. *Econ. Geol.*, 102(7): 1233-1267.
- Large R R, Bull S W and Maslennikov V V. 2011. A carbonaceous sedimentary source-rock model for Carlin-type and orogenic gold deposits[J]. *Econ. Geol.*, 106(3): 331-358.
- Li L, Santosh M and Li S R. 2015. The 'Jiaodong type' gold deposits: Characteristics, origin and prospecting[J]. *Ore Geology Reviews*, 65: 589-611.
- Li X H, Fan H R, Yang K F, Hollings P, Liu X, Hu F F and Cai Y C. 2018. Pyrite textures and compositions from the Zhuangzi Au deposit, southeastern North China Craton: Implication for ore-forming processes[J]. *Contributions to Mineralogy and Petrology*, 173 (73): 1-20.
- Lin Z W, Zhao X F, Xiong L and Zhu Z X. 2019. In-situ trace element analysis characteristics of pyrite in Sanshandao gold deposit in Jiaodong Peninsula: Implications for ore genesis[J]. *Advances in Earth Science*, 34(4): 399-413(in Chinese with English abstract).
- Maddox L M, Bancroft G M, Scaini M J and Lorimer J W. 1998. Invisible gold, comparison of Au deposition on pyrite and arsenopyrite[J]. *American Mineralogist*, 83(11-12): 1240-1245.
- Miao L C, Luo Z K, Huang J Z, Guan K, Wang G L, McNaughton J N and Groves I D. 1997. Zircon sensitive high resolution ion microprobe (SHRIMP) study of granitoid intrusions in Zhaoye gold belt of Shandong Province and its implication[J]. *Science in China (Series D: Earth Sciences)*, 40(4): 361-369.
- Möller P and Kersten G. 1994. Electrochemical accumulation of visible gold on pyrite and arsenopyrite surfaces[J]. *Mineralium Deposita*, 29: 404-413.
- Norris A and Danyushevsky L. 2018. Towards estimating the complete uncertainty budget of quantified results measured by LA-ICP-MS[C]. Goldschmidt: Boston, MA, USA.
- Peng H W, Fan H R, Liu X, Wen B J, Zhang Y W and Feng K. 2021. New insights into the control of visible gold fineness and deposition: A case study of the Sanshandao gold deposit, Jiaodong, China[J]. *American Mineralogist*, 106(1): 135-149.
- Peterson E C and Mavrogenes J A. 2014. Linking high-grade gold mineralization to earthquake-induced fault-valve processes in the Porgera gold deposit, Papua New Guinea[J]. *Geology*, 42(5): 383-386.
- Qiu Y M, Groves D I, McNaughton N J, Wang L G and Zhou T H. 2002. Nature, age, and tectonic setting of granitoid-hosted, orogenic gold deposits of the Jiaodong Peninsula, eastern North China Craton, China[J]. *Mineralium Deposita*, 37: 283-305.
- Reich M, Kesler S E, Utsunomiya S, Palenik C S, Chryssoulis S L and Ewing R C. 2005. Solubility of gold in arsenian pyrite[J]. *Geochimica et Cosmochimica Acta*, 69(11): 2781-2796.
- Reich M, Deditius A, Chryssoulis S, Li J W, Ma C Q, Parada M A, Barra F and Mittermayr F. 2013. Pyrite as a record of hydrothermal fluid evolution in a porphyry copper system: A SIMS/EMPA trace element study[J]. *Geochimica et Cosmochimica Acta*, 104: 42-62.
- Román N, Reich M, Leisen M, Morata D, Barra F and Deditius A P. 2019. Geochemical and micro-textural fingerprints of boiling in pyrite[J]. *Geochimica et Cosmochimica Acta*, 246: 60-85.
- Simon G, Huang H, Penner-Hahn J E, Kesler S E and Kao L S. 1999a. Oxidation state of gold and arsenic in gold-bearing arsenian pyrite[J]. *American Mineralogist*, 84(7-8): 1071-1079.
- Simon G, Kesler S E and Chryssoulis S. 1999b. Geochemistry and textures of gold-bearing arsenian pyrite, Twin Creeks, Nevada: Implications for deposition of gold in Carlin-type deposits[J]. *Econ. Geol.*, 94(3): 405-421.
- Song M C, Li S Z, Santosh M, Zhao S J, Yu S, Yi P H, Cui S X, Lü G X, Xu J X, Song Y X and Zhou M L. 2015. Types, characteristics and metallogenesis of gold deposits in the Jiaodong Peninsula, eastern North China Craton[J]. *Ore Geology Reviews*, 65: 612-625.
- Song M C, Song Y X, Ding Z J, Wei X F, Sun S L, Song G Z, Zhang J J, Zhang P J and Wang Y G. 2019. The discovery of the Jiaojia and the Sanshandao giant gold deposits in Jiaodong Peninsula and discussion on the relevant issues[J]. *Geotectonica et Metallogenesis*, 43(1): 92-110 (in Chinese with English abstract).
- Stefánsson A and Seward T M. 2004. Gold(I) complexing in aqueous

- sulphide solutions to 500°C at 500 bar[J]. *Geochimica et Cosmochimica Acta*, 68(20): 4121-4143.
- Tang J, Zheng Y F, Wu Y B, Gong B and Liu X M. 2007. Geochronology and geochemistry of metamorphic rocks in the Jiaobei terrane: Constraints on its tectonic affinity in the Sulu orogen[J]. *Precambrian Research*, 152(1-2): 48-82.
- Tang J, Zheng Y F, Wu Y B, Gong B, Zha X P and Liu X M. 2008. Zircon U-Pb age and geochemical constraints on the tectonic affinity of the Jiaodong terrane in the Sulu orogen, China[J]. *Precambrian Research*, 161(3-4): 389-418.
- Tanner D, Henley R W, Mavrogenes J A and Holden P. 2016. Sulfur isotope and trace element systematics of zoned pyrite crystals from the El Indio Au-Cu-Ag deposit, Chile[J]. *Contributions to Mineralogy and Petrology*, 171(33) : 1-17.
- Velasquez G, Beziat D, Salvi S, Siebenaller L, Borisova A Y, Pokrovski G S and de Parseval P. 2014. Formation and deformation of pyrite and implications for gold mineralization in the El Callao district, Venezuela[J]. *Econ. Geol.*, 109(2): 457-486.
- Wen B J, Fan H R, Hu F F, Liu X, Yang K F, Sun Z F and Sun Z F. 2016. Fluid evolution and ore genesis of the giant Sanshandao gold deposit, Jiaodong gold Province, China: Constrains from geology, fluid inclusions and H-O-S-He-Ar isotopic compositions[J]. *Journal of Geochemical Exploration*, 171: 96-112.
- Williams-Jones A E, Bowell R J and Migdisov A A. 2009. Gold in solution[J]. *Elements*, 5(5): 281-287.
- Xing Y L, Brugger J, Tomkins A and Shvarov Y. 2019. Arsenic evolution as a tool for understanding formation of pyritic gold ores[J]. *Geology*, 47(4): 335-338.
- Yang K F, Fan H R, Santosh M, Hu F F, Wilde S A, Lan T G, Lu L N and Liu Y S. 2012. Reactivation of the Archean lower crust: Implications for zircon geochronology, elemental and Sr-Nd-Hf isotopic geochemistry of Late Mesozoic granitoids from northwestern Jiaodong Terrane, the North China Craton[J]. *Lithos*, 146-147: 112-127.
- Yang L Q, Deng J, Wang Z L, Zhang L, Guo L N, Song M C and Zheng X L. 2014. Mesozoic gold metallogenic system of the Jiaodong gold Province, eastern China[J]. *Acta Petrologica Sinica*, 30(9): 2447-2467(in Chinese with English abstract).
- Yang L Q, Deng J, Wang Z L, Guo L N, Li R H, Groves D I, Danyushevsky L V, Zhang C, Zheng X L and Zhao H. 2016. Relationships between gold and pyrite at the Xincheng gold deposit, Jiaodong Peninsula, China: Implications for gold source and deposition in a brittle epizonal environment[J]. *Econ. Geol.*, 111(1): 105-126.
- Zhai M G and Santosh M. 2013. Metallogeny of the North China Craton: Link with secular changes in the evolving earth[J]. *Gondwana Research*, 24(1): 275-297.
- Zhu R X, Fan H R, Li J W, Meng Q R, Li S R and Zeng Q D. 2015. Detrinitic gold deposits[J]. *Science China-Earth Sciences*, 58(9): 1523-1537(in Chinese with English abstract).

附中文参考文献

- 范宏瑞, 冯凯, 李兴辉, 胡芳芳, 杨奎锋. 2016. 胶东-朝鲜半岛中生代金成矿作用[J]. 岩石学报, 32(10): 3225-3238.
- 郭敬辉, 陈福坤, 张晓曼, Siebel W, 翟明国. 2005. 苏鲁超高压带北部中生代岩浆侵入活动与同碰撞—碰撞后构造过程: 锆石 U-Pb 年代学[J]. 岩石学报, 21(4): 1281-1301.
- 林祖伟, 赵新福, 熊乐, 朱照先. 2019. 胶东三山岛金矿床黄铁矿原位微区微量元素特征及对矿床成因的指示[J]. 地球科学进展, 34 (4): 399-413.
- 宋明春, 宋英昕, 丁正江, 魏绪峰, 孙绍立, 宋国政, 张军进, 张丕建, 王永国. 2019. 胶东焦家和三山岛巨型金矿床的发现及有关问题讨论[J]. 大地构造与成矿学, 43(1): 92-110.
- 杨立强, 邓军, 王中亮, 张良, 郭林楠, 宋明春, 郑小礼. 2014. 胶东中生代金成矿系统[J]. 岩石学报, 30(9): 2447-2467.
- 朱日祥, 范宏瑞, 李建威, 孟庆任, 李胜荣, 曾庆栋. 2015. 克拉通破坏型金矿床[J]. 中国科学: 地球科学, 45(8): 1153-1168.